Thin Solid Films 759 (2022) 139466

Contents lists available at ScienceDirect

Thin Solid Films

journal homepage: www.elsevier.com/locate/tsf

Surfaces, Interfaces and Colloidal Behaviour

Towards Ge-based electronic devices: Increased longevity of alkanethiol-passivated Ge(100) in low humidity environments

Shane Garvey [a,c], Andrew Serino [d,*], Maria Barbara Maccioni [a], Justin D. Holmes [a,b], Michael Nolan [a], Nerissa Draeger [d], Emir Gurer [d], Brenda Long [a,*]

[a] School of Chemistry, University College Cork, Cork T12 YN60, Ireland
[b] AMBER Centre, Environmental Research Institute, University College Cork, Cork T23 XE10, Ireland
[c] Tyndall National Institute, University College Cork, Cork T12 R5CP, Ireland
[d] Lam Research Corp., Fremont, CA 94538, USA

ARTICLE INFO

Keywords:
Germanium
Humidity
Passivation
Self-assembled monolayers
Stability
X-ray photoelectron spectroscopy

ABSTRACT

Germanium is a critically important material for future complementary metal-oxide-semiconductor devices, however, to maximise its potential it is necessary to develop a robust passivation process that prevents Ge re-oxidation for a queue time of 24 h. Self-assembled monolayers (SAMs) of alkanethiols on Ge have previously been shown to inhibit oxidation; however, re-oxidation eventually occurs when exposed to ambient conditions. Herein, it is shown that humidity plays a key role in the degradation of the SAM, ultimately resulting in re-oxidation. To demonstrate this, thiol-passivated Ge(100) surfaces are exposed to controlled humidity environments with different levels of relative humidity (RH). The rate of re-oxidation of the Ge surfaces are tracked using X-ray photoelectron spectroscopy and water contact angle analysis to discern what role RH plays in the re-oxidation of the Ge and the degradation of the SAM passivation. Atomic force microscopy data is presented to show that humidity-mediated re-oxidation of the Ge has little or no impact on the route mean square roughness of those surfaces. Finally, atomistic modelling of thiol-SAM passivated Ge in the presence of water molecules has been studied using first principles density functional theory in order to simulate experimental conditions and to understand the atomic level processes that determine stability in hydrophilic and hydrophobic configurations.

1. Introduction

Traditionally, Si was used as the semiconductor material of choice due to its relative abundance [1] and mechanical strength [2], but most importantly because of its stable native oxide and very good oxide/Si interface [3]. However, as aggressive device-scaling has continued, traditional dielectrics such as SiO_2 have become ineffective at insulating the channel from the gate [4]. At such small dimensions, electrons can tunnel through the gate oxide resulting in high leakage currents and poor device performance [5,6]. As a result, there has been a shift from traditional dielectrics to high-κ dielectrics such as HfO_2 and ZrO_2 in an effort circumvent the aforementioned tunneling issue [7]. Regardless, continued transistor scaling has been driving efforts to find higher mobility semiconductor materials with properties suited to the modern demands of complementary metal oxide semiconductor (CMOS) device fabrication and performance. Other high mobility materials such as III-V semiconductors [8,9] and two-dimensional transition metal dichalcogenides [10,11] are being scrutinized for their potential use in future devices also.

Germanium, however, is a very attractive alternative for a number of reasons. Critically, it boasts an electron and hole mobility more than twice and four times that of silicon (Si), respectively, and its similarity to Si, as another Group IV element, would allow it to be seamlessly incorporated using similar fabrication processes. The global reserves of Ge are estimated to be approximately 2-3 thousand tons [12]. By comparison, Si as the second most abundant element in the earth's crust, has an annual production of approximately 7 million tons. Given these relative abundances it is unlikely that Ge will replace Si entirely. However, it is plausible that Ge will be integrated into the Si platform as the channel material and efforts to do such are well underway [13–15]. Current transistor manufacturing includes channels consisting of silicon-germanium (SiGe alloys to gain the partial benefits of Ge. In

Abbreviations: SAM, Self-assemble monolayer; XPS, X-ray photoelectron spectrocscopy.

* Corresponding authors.
E-mail addresses: Andrew.Serino@gmail.com (A. Serino), brenda.long@ucc.ie (B. Long).

https://doi.org/10.1016/j.tsf.2022.139466
Received 1 December 2021; Received in revised form 31 August 2022; Accepted 1 September 2022
Available online 5 September 2022

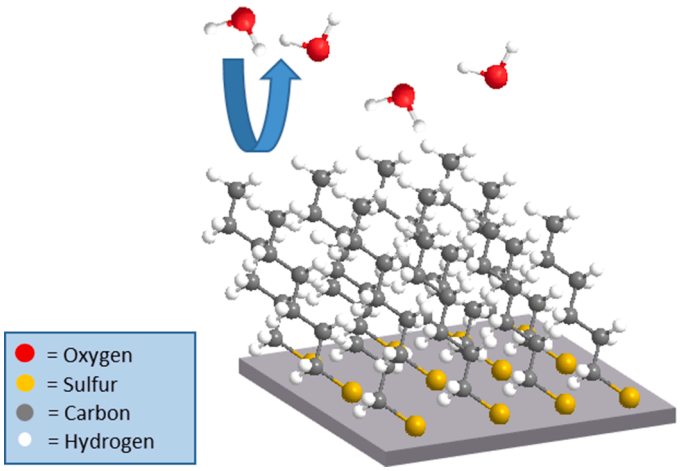

Fig. 1. Schematic of thiol-SAM on Ge.

2020, Intel published results for a gate-all-around nanosheet p-channel, enhancement mode metal–oxide–semiconductor field-effect transistors transistor using $Si_{0.4}Ge_{0.6}$ [16].

A contributing factor as to why pure Ge has not yet been integrated into current devices is that Fermi level pinning of the Ge surface occurs when contacting a metal due to unpassivated acceptor-like gap states present at the interface [17,18]. Dimoulas et al. have hypothesized that since the Fermi level in Ge lies higher than the charge neutrality level, the gap states at the interface fill easily, building up a fixed negative charge preventing efficient inversion in the inversion layer of the CMOS device resulting in sub-optimal device performance [19]. Many of the other issues with Ge are specifically related to the nature of the oxide. For example, the Ge/GeO_2 interface is characterized by interfacial dangling bonds and vacancies which trap charge, hindering device performance [20,21]. Also, significant GeO desorption occurs at the high temperatures necessary to grow high quality GeO_2 films on Ge whereas this is not the case with the Si system [22]. The desorption of GeO during thermal oxidation affects the qualities of both the Ge/GeO_2 interface and the bulk GeO_2 itself. With that said, Toriumi et al. have performed Ge oxidation under high-pressure O_2 conditions at high temperatures to suppress the GeO desorption and avoid deteriorating the GeO_2 bulk film quality or Ge/GeO_2 interface [23]. Finally, GeO_2 is water soluble, making it extremely problematic for aqueous wafer-processing steps which are currently common in device manufacturing [24]. In fact, native oxide etching of GeO_2 using water, results in the formation of the suboxide, GeO_x, which can then be removed by annealing at temperatures above 450°C leaving a pristine Ge surface [25]. However, upon exposure to ambient conditions, the native oxide readily regrows. For the reasons outlined, when working with Ge, it may be advantageous to remove the native oxide and to store the oxide-free Ge under an inert atmosphere, ultra-high vacuum conditions. However, we show that a simple surface chemistry will passivate Ge to ensure no oxide regrowth occurs over a 24 h period.

Many methods to passivate Ge have been explored and are discussed in the scientific literature – these include both wet and dry methods of passivation using halides [26–28], carboxylic acids [29], sulfur [30], nitride [31], oxynitride [32] passivation by graphene [20,33,34], and self-assembled monolayers (SAMs) [35,36]. SAMs have been the subject of extensive research throughout the latter half of the 20th century and well into the 21st, as it is understood that organic functionalization of surfaces can dramatically affect the properties of those surfaces. The early literature on SAMs focused on their assembly onto planar gold [37]; however, since then the study of SAMs has expanded to many other materials such as copper [38,39], bismuth [40], graphene [41], III-Vs

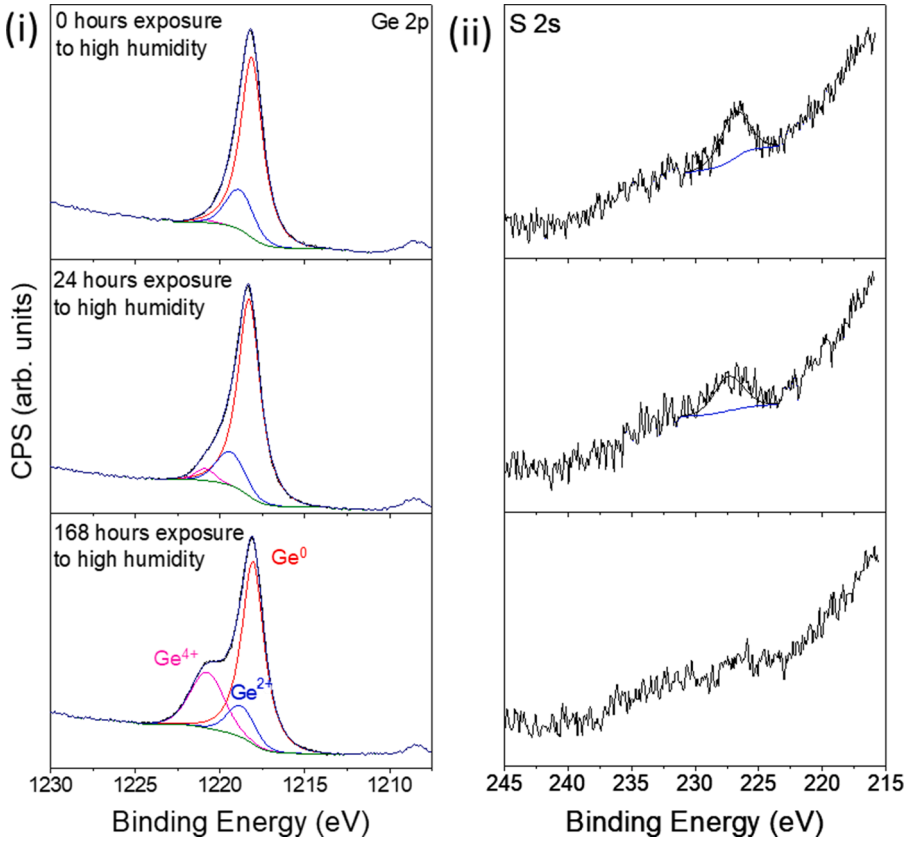

Fig. 2. (i) Ge 2p and (ii) S 2s spectra for HT-passivated Ge showing increasing in intensity of GeO_2 peak and decrease in intensity of sulfur peak for the sample exposed to 90% RH over 168 h.

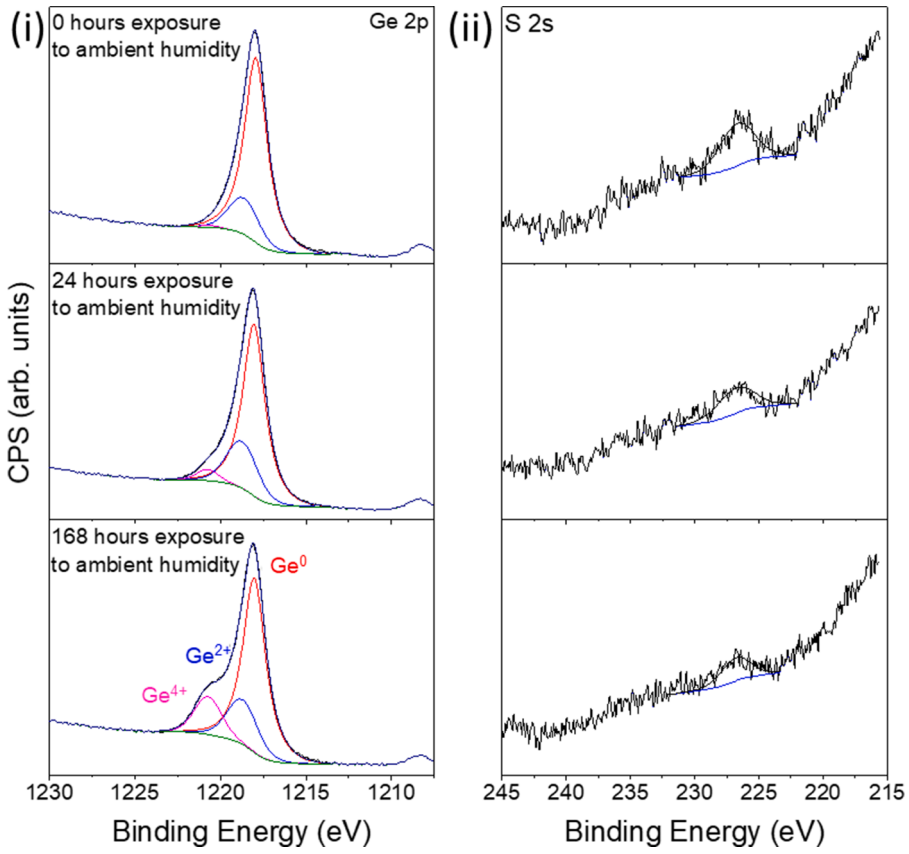

Fig. 3. (i) Ge 2p and (ii) S 2s spectra for HT-passivated Ge showing increase in intensity of GeO_2 peak and decrease in intensity of S peak for ambient humidity sample over 168 h.

[42, 43] and semiconductors such as Si, SiGe and Ge [35,43]. A SAM is formed through the adsorption of molecules onto a surface, followed by a period of organization whereby the adsorbate molecules rearrange themselves to form a system that is energetically favorable. This results in a self-limiting process that minimally impacts the substrate but enables the alteration of surface properties such as the wettability and oxidation resistance [35,36]. There are myriad reasons to form organic monolayers on the surfaces of semiconductor materials [44]; however, some examples include; for mono-layer doping [45–48], to enhance the stability and efficiency of solar cells [49,50] and for electrochemical sensors [51].

Several studies have explored the use of alkanethiol SAMs for inhibiting oxide growth on germanium, however, reported stabilities are widely variable [36,52–54]. Previously, we have documented a method to achieve the vapor-phase passivation of Ge(100) using 1-hexanethiol (Fig. 1) [36]. Herein, we investigate the role that the environment, specifically humidity, plays in the stability of SAM-passivated Ge and subsequent Ge oxidation using three different alkanethiol-Ge systems. In this study, thiol SAMs are used to passivate Ge(100) surfaces which are then placed in a controlled humidity environment with different levels of RH. Understanding the mechanism for surface instability is crucial for SAMs to gain industry adoption for Ge oxide control.

2. Method and materials

2.1. Preparation of SAMs on Ge surfaces

Samples were prepared by three different methods, (i) vapor-phase deposition of 1-hexanethiols, (ii) vapor-phase deposition of 1-octanethiols, and (iii) solution-phase deposition of 1-dodecanethiols. The first method was conducted in an academic setting and used for identifying a humidity trend, the latter two were conducted in an industrial setting. No direct comparisons were made between the two settings.

2.1.1. Vapor-phase deposition of 1-hexanethiols

Passivation of the Ge(100) surface was achieved using vaporized 1-hexanethiol (HT) using a method previously outlined by the authors. The passivated Ge coupons were exposed to air in low (5%), ambient (40%) and high (90%) RH environments for 168 h to determine what effect the water vapor in air had on the Ge surfaces. For the purposes of this study, the humidity-controlled environment with 40% RH is referred to as 'ambient humidity'. In an attempt to isolate the water vapor from the low humidity environment without also isolating O_2, compressed air (which has a low water content) was used. In this case, Ge coupons were held in a glass vessel filled with desiccant through which compressed air was flowed continuously. A humidity sensor was used to track the humidity in the glass vessel. For both the ambient and high humidity tests, a Vötsch humidity-controlled chamber was used. In all cases, the samples were exposed to a constant temperature of 20°C. After 24 and 168 h in their respective environments, samples were characterized using atomic force microscopy (AFM), water contact angle (WCA) and X-ray photoelectron spectroscopy (XPS)

2.1.2. Vapor-phase deposition of 1-octanethiols

Coupons of Ge(100) were etched with an hydrochloric acid (HCl) based proprietary etch designed to remove surface oxides and contaminants and provide a temporary Cl termination, and dried under a nitrogen gas stream. Samples were transferred to a custom low-pressure vacuum deposition chamber, with a transfer time up to 5 min. 1-octanethiol (OT) was deposited using vapor draw at 80° C and 107 Pa for 3 cycles of 10 minute doses. Samples were removed and rinsed with

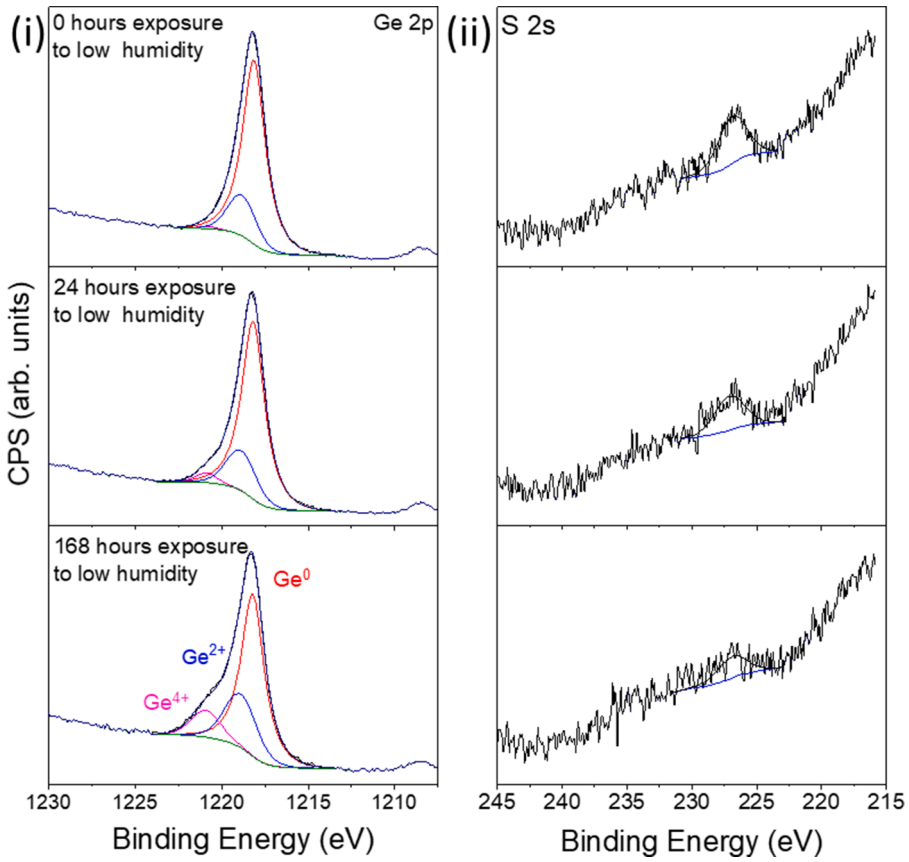

Fig. 4. (i) Ge 2p and (ii) S 2s spectra for HT-passivated Ge showing increase in intensity of GeO_2 peak and decrease in intensity of sulfur peak for sample exposed to 5% RH over 168 h.

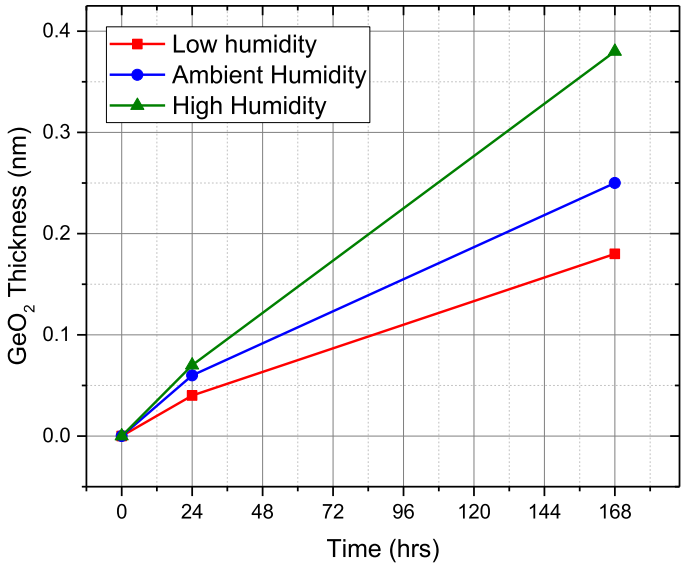

Fig. 5. GeO_2 thicknesses of HT-passivated Ge exposed to low, ambient, and high RH for 0, 24 and 168 h.

anhydrous ethanol, dried under a nitrogen stream, and immediately placed in target environments. The passivated Ge coupons were exposed to low (5%) and ambient (~40%) RH environments for 24 h at room temperature and analyzed by XPS. For the low humidity case, Ge coupons were held in a vessel filled with desiccant. A humidity and oxygen sensor was used to monitor the humidity and oxygen levels to ensure consistency.

2.1.3. *Liquid-phase deposition of 1-dodecanethiols*

Coupons of Ge(100) and $Si_{0.25}Ge_{0.75}$(100) (SiGe75) were etched with the same HCl based proprietary etch as vapor deposition of OT. Samples were immediately transferred to a solution of 25 mM 1-dodecanethiol (DDT) in anhydrous ethanol at room temperature. After 24 h samples were removed and rinsed with anhydrous ethanol, dried under a nitrogen stream, and immediately placed in target environments. The passivated Ge coupons were exposed to low (5%) and ambient (~40%) RH environments at room temperature for 24 h and analyzed by XPS. For the low humidity case, Ge coupons were held in a vessel filled with desiccant. A humidity and oxygen sensor were used to monitor the humidity and oxygen levels to ensure consistency.

2.2. *Characterization methods*

All AFM measurements were taken using tapping mode Veeco Multimode V at room temperature over a 3 x 3 μm^2 scanning area.

For WCA, an image of a 50 μL drop of deionized water on the Ge surface was obtained and the angle formed between the water, Ge surface, and air was measured.

XPS measurements were carried out on two instruments. Vapor-phase deposited hexanethiol samples were analyzed using an Oxford Applied Research Escabase XPS System with a CLASS VM 100 mm mean radius hemispherical electron energy analyzer with multichannel detectors in an analysis chamber with a base pressure of 5.0×10^{-7} Pa. Survey scans were swept twice and were acquired using a pass energy of 50 eV, a step size of 0.7 eV and a dwell of 0.3 s. All core level scans, were averaged over 10 scans and were acquired with a step size of 0.1 eV, a dwell time of 0.1 s and a pass energy of 20 eV except for the S 2s, which

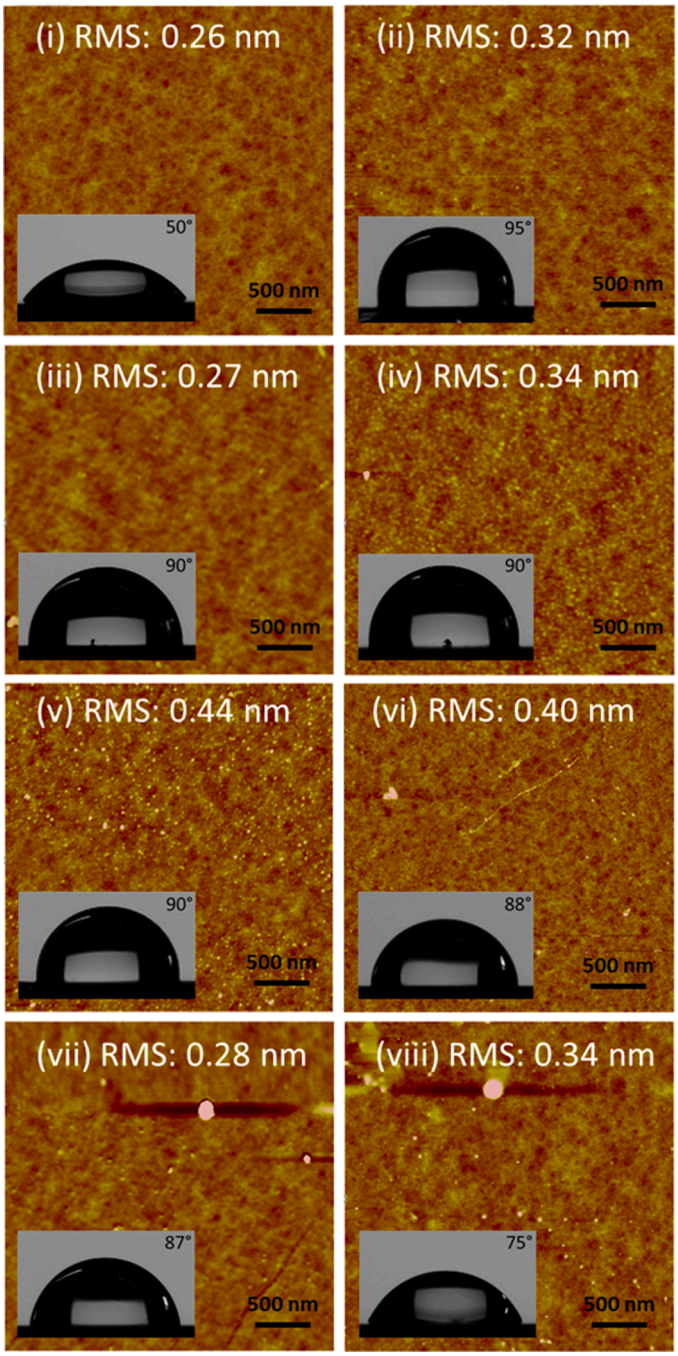

Fig. 6. WCA and AFM data for (i) as-rec Ge (ii) HT-passivated Ge (iii) and (iv) HT-passivated Ge with 24 and 168 h exposure to the low humidity environment respectively, (v) and (vi) HT-passivated Ge with 24 and 168 h exposure to the ambient humidity environment respectively, (vii) and (viii) HT-passivated Ge with 24 and 168 h exposure to high humidity environment respectively.

was acquired with a pass energy of 50 eV averaged over 20 scans. This was done to maximize the intensity of the sulfur peaks to allow for accurate peak fitting. A non-monochromated Al-Kα X-ray source (1486.58 eV) at 100 W power (10 mA, 10 kV) was used for all scans.

Vapor-phase deposited OT and solution-deposited DDT samples were analyzed using a ThermoFisher Scientific Theta 300 at 1 x 10^{-7} Pa with a monochromatic Al-Kα source at 100 W (6.67 mA and 15 kV) with a 400 μm spot size. A pass energy of 50 eV was used to collect high energy resolution spectra with a step size of 0.1 eV, a dwell time of 50 ms, and 15, 15, and 20 sweeps for C 1, Ge 2p, and S 2s, respectively.

All spectra were acquired at a take-off angle of 90° with respect to the analyzer axis and were charge corrected with respect to the C 1s photoelectric line at 284.8 eV. A Shirley type background was used for construction and peak fitting of synthetic peaks. Synthetic peaks were a mix of Gaussian-Lorenzian; the Ge 2p spectra were fit using Gaussian-Lorentzian peak shape GL(90) for the elemental Ge peak and Lorentzian peak shape LA(1.53,243) for all other peaks. The relative sensitivity factors used are from a CasaXPS library containing Scofield cross-sections.

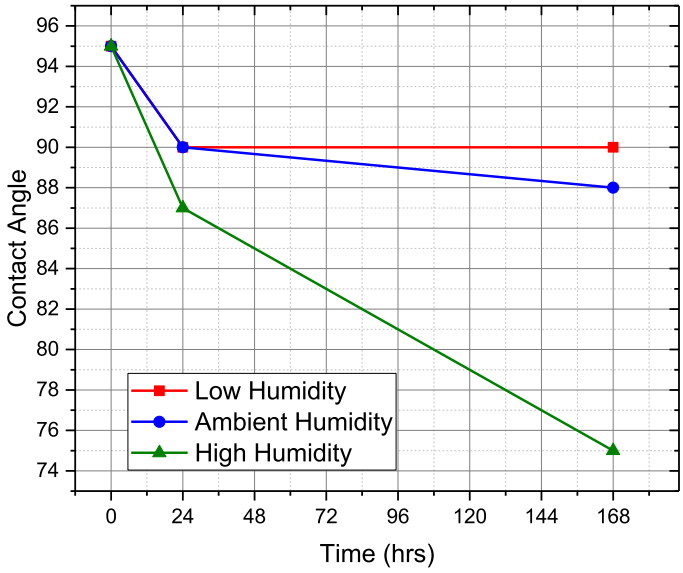

Fig. 7. WCA data for HT-passivated Ge plotted against time spent in respective RH environments. WCA for as-received Ge is 50° [62].

2.3. First principles density functional theory simulations

DFT calculations as implemented in the Vienna Ab Initio Software Package [55,56] have been used to model alkanethiol SAMs on the Ge (100) surface and to explore how humidity could influence Ge surface passivation. The calculations utilize a plane wave basis set in a 3-dimensional periodic slab model of the substrate with DFT-optimized lattice constants. The core electrons are described by projector augmented wave [57] potentials and the exchange and correlation energies are modelled according to the generalized gradient approximation with the Perdew-Burke-Ernzerhof (PBE) [58] gradient corrected functional. In order to take into account the van der Waals interactions between alkanethiols and water, we used the DFT-D3 dispersion correction method [59] that incorporates the long-range dispersion contribution to the exchange-correlation PBE functional. We use the following valance electron configurations; for germanium; Ge $4s^2$ and $4p^2$, for chlorine; Cl $3s^2$ and $3p^5$, for sulfur; S $3s^2$ and $3p^4$, for carbon; C$2s^2$ and $2p^4$, for oxygen; O $2s^2$ and $2p^4$, and for hydrogen; H $1s^1$. All the calculations were executed using an energy cut-off for the valence electron plane wave basis set at 420 eV and the convergence criteria for electronic relaxations and ionic relaxations at 10^{-4} eV and 0.02 eV/Å respectively. The Brillouin zone was sampled with (2 × 2 × 1) Monkhorst-Pack k-point grids [60].

3. Results and discussion

3.1. Impact of humidity on SAM-Ge stability

The primary characterization method for the study of SAM degradation and Ge oxidation is XPS since it gives accurate determination of elemental composition and oxidation states of those elements at the surface (~10 nm sampling depth) of the samples being characterized. As

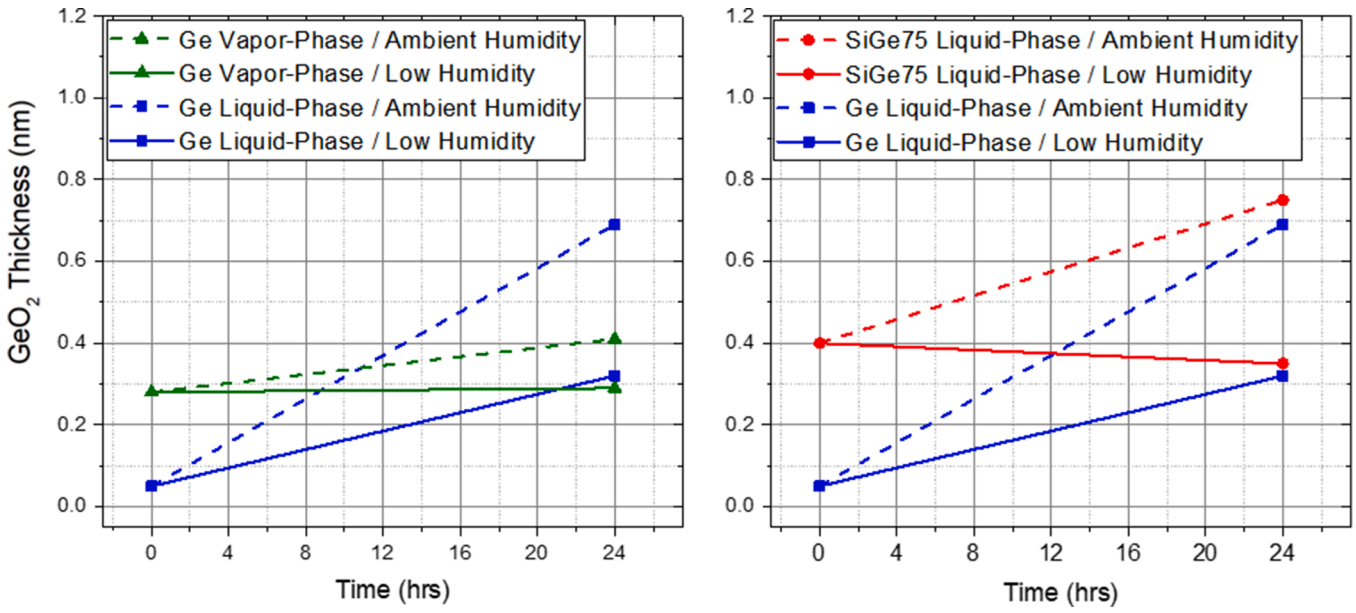

Fig. 8. GeO_2 thicknesses of (left) Ge samples passivated by vapor-phase deposited OT and solution-phase deposited DDT and (right) DDT-passivated SiGe75 exposed to low and ambient RH for 0 and 24 h. Values extracted from Ge 2p spectra.

such, the growth of GeO_2 was tracked as a function of exposure time to different levels of RH. For the purposes of this study, Ge 2p spectra from XPS were used to track oxidation of the Ge(100) surfaces since the Ge 2p transition is more surface sensitive than Ge 3d. In addition, to track the presence of sulfur, the S 2s spectra were acquired. The authors have previously published XPS spectra for HCl-etched Ge(100) [36]. Oxide thickness was calculated using the method outlined previously by Murakami et al. [61].

$$d_{GeO_2} = \lambda_{GeO_2} sin\theta \, ln\left(\frac{I^{\infty}_{Ge}}{I^{\infty}_{GeO_2}}\frac{I_{GeO_2}}{I_{Ge}} + 1\right)$$

Where λ_{GeO_2} is the inelastic mean free path for the Ge 2p transition, which is 0.9 nm; the photoemission angle θ is 90°; $I^{\infty}_{Ge}/I^{\infty}_{GeO_2}$ is the ratio of the Ge 2p signal from infinitely thick Ge to infinitely thick GeO_2 and is 1.73 and 3.25 for the Oxford Applied Research and ThermoFisher instruments, respectively; I_{GeO_2} is the intensity of the of native oxide (GeO_2) peak from curve fitting the Ge 2p feature; I_{Ge} is the intensity of the bulk Ge peak from curve fitting the Ge 2p transition. This calculation was repeated to determine the thickness of the suboxide (GeO_x) component for each sample. In this case, I_{GeO_x}, the fraction of suboxide (GeO_x) from curve fitting the Ge 2p was used in place of I_{GeO_2}.

In Fig. 2 (i), the Ge 2p XPS spectra for HT-passivated Ge with 0, 24 and 168 h of exposure to the high RH environment is shown. Directly after the passivation reaction, after 0 h of exposure, only the peaks corresponding to Ge^0 at 1218.2 eV (red) and Ge^{2+} at 1219.3eV (blue) are present. There is no peak corresponding to Ge^{4+} since the initial HCl etch has effectively removed the original native oxide and the subsequent passivation procedure has prevented re-growth of native oxide. As stated, there is a contribution from Ge in a +2 oxidation state (blue). This contribution is likely present due to a combination of the suboxide (GeO) and Ge bonded to S after the passivation reaction. A peak separation of 1.1 eV between the Ge^0 and Ge^{2+} components was observed for the sample with 0 h exposure to high humidity. In Fig. 2 (ii), the S 2s peak at 226.9 eV after 0 h of exposure is also displayed. Here, a clear S signal is observed which confirms that the thiol molecules have bonded to the Ge surface. Upon exposure to the high humidity environment for 24 h, an increase in the intensity of the GeO_2 peak at 1220.9 eV (pink) is observed in the Ge 2p spectrum and after 168 h, a greater increase in peak intensity is observed with the peak shifting slightly (0.05 eV) to higher binding energy as the GeO_2 film thickness increases from 0.07 nm after 24 h to 0.38 nm after 168 h. Also, the S 2s signal decreases in intensity from 0 to 24 h of exposure indicating that some of the thiol molecules have been displaced from the Ge surface. After 168 h, S is no longer detectable by XPS indicating that the majority of the SAM has been displaced by oxide. The changes observed in the XPS over 168 h of exposure to the high RH environment can be contextualized and the role water vapor has on the thiol-passivated Ge can be understood when the same measurements are taken for samples exposed to lower levels of humidity over the same period of time.

In Fig. 3, the Ge 2p (i) and S 2s (ii) XPS data for the HT-passivated Ge which was exposed to ambient humidity for 168 h is shown. As was observed with the high humidity samples, there is no GeO_2 present directly after the passivation reaction and after 24 h of exposure to the ambient the GeO_2 thickness is calculated to be 0.06 nm. After 168 h of exposure the ambient, the GeO_2 peak at 1220.8 eV increases in intensity and the oxide thickness is calculated to be 0.25 nm. While there is a growth of GeO_2 in 168 h, there is also a loss of S as can be seen in Fig. 3 (ii), whereby the S 2s peak diminishes within the first 24 h and over the following 144 h. There is still detectable S even after the 168 h period. These results differ from the high humidity samples. For one, there is less GeO_2 growth over the 168 h exposure period, with an oxide thickness of 0.25 nm compared to a thickness of 0.38 nm at high humidity, and S is still detectable on the surface over that same period – an indication that the SAM is still present and maintaining oxidation resistance to the Ge surface.

To complete the picture, passivated Ge surfaces were exposed to a low humidity environment and again, characterized by XPS. In Fig. 4, the Ge 2p (i) and S 2s (ii) XPS plots for the sample exposed to the low humidity environment are displayed. After 24 h of exposure to the low RH environment, there is 0.04 nm of GeO_2 growth and a slightly reduced intensity S 2s peak when compared with that after 0 h of exposure. After 168 h, 0.18 nm of the native oxide has grown and S is still detectable by XPS on the surface. The XPS data from Figs. 2, 3 and 4 combine to reveal what effect humidity has on the surface of the Ge. It is apparent that in the presence of water vapor, the passivated Ge begins to oxidize over time and the amount of S on the surface decreases as the thiol molecules desorb from the surface. The progressive growth in GeO_2 for each sample set is displayed in Fig. 5.

It is clear from Fig. 5 that oxidation of the Ge surface trends with

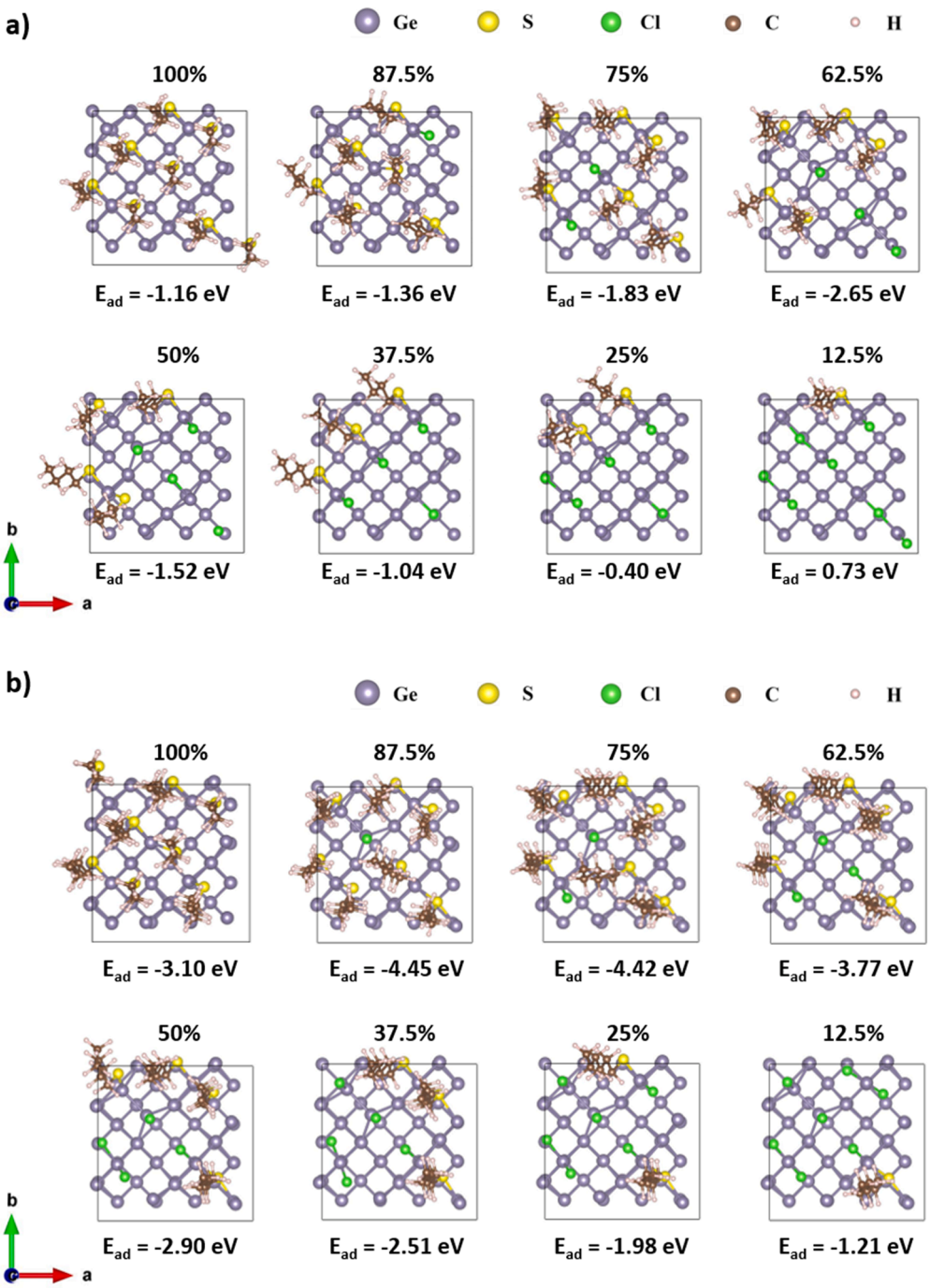

Fig. 9. Atomic structures of (a) butanethiol and (b) hexanethiol on Ge(100) at different coverages, with respective computed adsorption energies.

humidity. It was not possible to achieve a 0% RH environment in air at 20°C and therefore the growth of oxide observed for the low RH case can be attributed to the small but non-negligible amount of water vapor in the air.

WCA analysis was carried out on each sample directly after the passivation procedure and after 24 and 168 h in their respective environments. This is a qualitative measurement technique that gives an indication of the wettability of a surface. The wettability of the Ge surface is affected by how the surface is terminated. For example, the as-received Ge surface with its native oxide film interacts favorably with water, resulting in a hydrophilic surface and a shallow contact angle between the water droplet, Ge, and air. When the oxide is replaced with the methyl-terminated monolayer, a more hydrophobic termination, the polar water molecules in the droplet interact less favorably and thus do not wet the surface, resulting in a steep contact angle between water, Ge and air. In Fig. 6 (ii), a contact angle of 95° is measured for the HT-passivated Ge. By tracking the changes in the angle of the water droplet with the substrate and air, we gain insights into how exposure to the environment with different levels of RH affects the presence of the SAM. The WCA for the sample exposed to the low humidity environment decreases by 5° in 24 h but does not decrease further in the following 144 h (Fig. 6 (iii) and (iv)). A similar result is observed for the sample exposed to the ambient humidity – a decrease of 5° in the WCA is observed in the first 24 h of exposure to the ambient and over the next 144 h of exposure, the contact angle only decreases by a further 2°.

The largest change in contact angle is observed for the sample

Table 1
Calculated interaction energies of Ge(100) surface with full coverage of alkanethiolates at different concentration of water molecules. The two energies presented for each thiolate are the total interaction energy for *n* water molecules and the interaction energy per water molecule.

	Butanethiol on Ge(100) at 100%		Hexanethiol on Ge(100) at 100%	
n H_2O	E_{int} (eV)	E_{int} /n (eV)	E_{int} (eV)	E_{int} /n (eV)
1	-0.09	-0.09	-0.09	-0.09
2	-0.39	-0.19	-0.48	-0.24
3	-0.82	-0.27	-0.84	-0.28
4	-1.38	-0.35	-1.36	-0.34
5	-1.73	-0.35	-2.24	-0.45
6	-2.08	-0.35	-2.18	-0.36
7	-3.26	-0.47	-2.67	-0.38
8	-3.66	-0.46	-3.63	-0.45

exposed to the high humidity environment for 168 h. In this case, the WCA drops by 8° over the first 24 h and by a further 13° in the following 144 h (Fig. 6 (vii) and (viii)). Over the 168 hour period of exposure to the high humidity environment, the WCA decreased by a total of 22°. This indicates that the longer-term stability of the SAM is influenced greatly by the exposure to the high humidity environment.

Taking this result together with the XPS results in Fig. 2 elucidates how the water vapor damages the SAM, allows surface oxidation, and promotes an increase in the intensity of the peaks corresponding to GeO_2. A summary of the WCA results are displayed in Fig. 7. The AFM images in Fig. 6 show what effect, if any, exposure to the respective environments had on the surface roughness of the Ge. A pristine surface with roughness RMS value of 0.26 nm is observed for degreased Ge (Fig. 6 (i)). For all other samples, an increase in surface roughness is observed and for the samples exposed to the high relative humidity, some spots are observed that may be oxide formations on the Ge surface at point defects.

Previous reports explored the stability of DDT SAMs that were deposited on Ge(100) through solution-phase passivation. To demonstrate further the role of humidity in that work, the growth of GeO_2 over time in low and ambient humidity environments for alkanethiol SAMs formed by vapor-phase passivation is compared to that of solution-phase passivation in Fig. 8. Due to the difficulty of depositing DDT by vapor, which is a result of the molecule's high vapor pressure, OT is used, which is a similar long chain alkyl-thiol but has a lower vapor pressure. The dry deposition shows a similar trend to the vapour phase SAM deposition, with a GeO_2 thickness is 0.01 and 0.13 nm for low and ambient humidity environment samples, respectively. This trend continues for solution-phase passivation where the thickness of GeO_2 is 0.25 and 0.64 nm for low and ambient humidity environment samples, respectively. These data also suggests that deposition method, and thus SAM quality, plays a role in stability as well-ordered, hydrophobic alkyl-backbones contribute to preventing water molecules from reaching the SAM-Ge interface.

While the goal is to eventually replace Si with pure Ge in devices, $Si_{1-x}Ge_x$ is the current alternative. As the percentage of Ge increases in SiGe alloys, the native oxide challenges associated with the native oxide of Ge become more pronounced. Today, mainstream logic devices in high volume manufacturing are limited to <60% Ge. In Fig. 8, solution-phase passivation of DDT on SiGe75 (25:75 Si:Ge) is shown. The GeO_2 thickness is 0.05 and 0.35 nm for low and ambient humidity, respectively. While the data suggests a decrease in GeO_2 for the low humidity sample, it is likely a result of sample variation. The growth of GeO for SiGe75 in ambient humidity and the lack of growth for low humidity indicates that the role humidity plays follows the same trends for SiGe alloys as for pure Ge. By controlling for humidity, SAM stability on SiGe can be increased, thus reducing the amount of germanium oxide growth.

3.2. Modelling SAM passivation of Ge surfaces and the impact of humidity

DFT calculations were performed to understand the atomic level detail of the SAM stability and the interaction between SAMs and water molecules. We use extensive static relaxations to explore how water interacts with SAMs and at the Ge-SAM interface. While ab initio molecular dynamics would be useful to explore this in more detail, such analysis requires significant calculations beyond the scope of this work.

The Ge(100) surface is modelled with a (2x2) surface supercell expansion with 128 atoms while the 40 Å of vacuum separating the slabs along the periodic direction perpendicular to the surface allows for a range of alkanethiol chain lengths from two to twelve carbon atoms to be explored while removing periodic interactions perpendicular to the surface. To simulate the conditions of the bulk, Ge atoms in the bottom layer of the slab are fixed. The top surface, composed by 8 Ge atoms, was initially fully passivated with Cl atoms.

We first determine the stable structures of alkanethiols on Ge and then we explore the influence of humidity for the SAMs with 4 and 6 carbon atom backbones as these are computationally tractable. The search for the most stable interface structure of the SAM on Ge was carried out by calculating the adsorption energy of these alkanethiols on Ge surfaces at various coverages. With 8 Ge atoms in the outermost (terminal) surface layer, coverages from 12.5 % to 100 % can be constructed.

The adsorption energy of the thiols at the Ge(100) surface is computed with adsorption in the thiolated form, in which the S–H bond breaks during adsorption onto the Ge surface, and leads to HCl formation. We calculated the adsorption energies (E_{ads}) with the following expression:

$$E_{ad} = E(tot) + E(nHCl) - [E(Cl:Ge) + E(nHS - C_xH_{2x+1})]$$

where E(tot) is the total energy of the thiol-functionalized Ge surface, with *n* adsorbed thiol molecules, E(*n* HCl) is the energy of the isolated HCl molecule multiplied by the number, *n,* of HCl molecules, E (Cl:Ge) is the energy of the Cl passivated Ge(100) surface and E (nHS-C_xH_{2x+1}) is the energy of *n* alkanethiol molecules. All the energies have been computed using the same parameters including the van der Waals corrections [59].

We have examined different coverages and arrangements of the thiol molecules on Ge(100) for the examples of C_4 and C_6 alkanethiolates. The relaxed structures of the most stable butane- and hexanethiol-passivated Ge(100) surfaces at different coverages and the respective adsorption energies are reported in Fig. 9. These stable thiolate coverages are used as models for humidity explorations.

For C_4 and C_6 alkanethiols, the most favorable coverages on the Ge (100) surface are 62.5% for C_4 and 87.5% for C_6, with computed adsorption energies of -2.65 eV and -4.45 eV respectively; we see that the C_6 thiolate chain shows a stronger interaction with the Ge(100) surface, which can be attributed to the alkyl chain-chain interactions that are stronger for longer thiol chains. A detailed discussion of the stability and structure of a wide range of thiolate SAMs on Ge(100) will be presented in another paper.

In Table 1, we present computed interaction energies of water at butane- and hexanethiol-passivated Ge at full SAM coverage. For each SAM, two energies are presented – E_{int} is the interaction energy relative to *n* water molecules ($n = 1 - 8$), while E_{int} / n is the interaction energy per water molecule divided by the number of water molecules.

From Table 1, the magnitude of the interaction energy increases with the number of water molecules. However, the computed interaction energy per molecule is relatively constant, around -0.25 ± 0.05 eV for low concentration ($n = 2–4$) and -0.40 ± 0.05 eV for high concentration (n = 5 - 8) in both SAM-Ge systems and therefore the influence of the chain length on the interaction with water is constant for these thiolate chains. This is most likely due to the presence of the terminating methyl

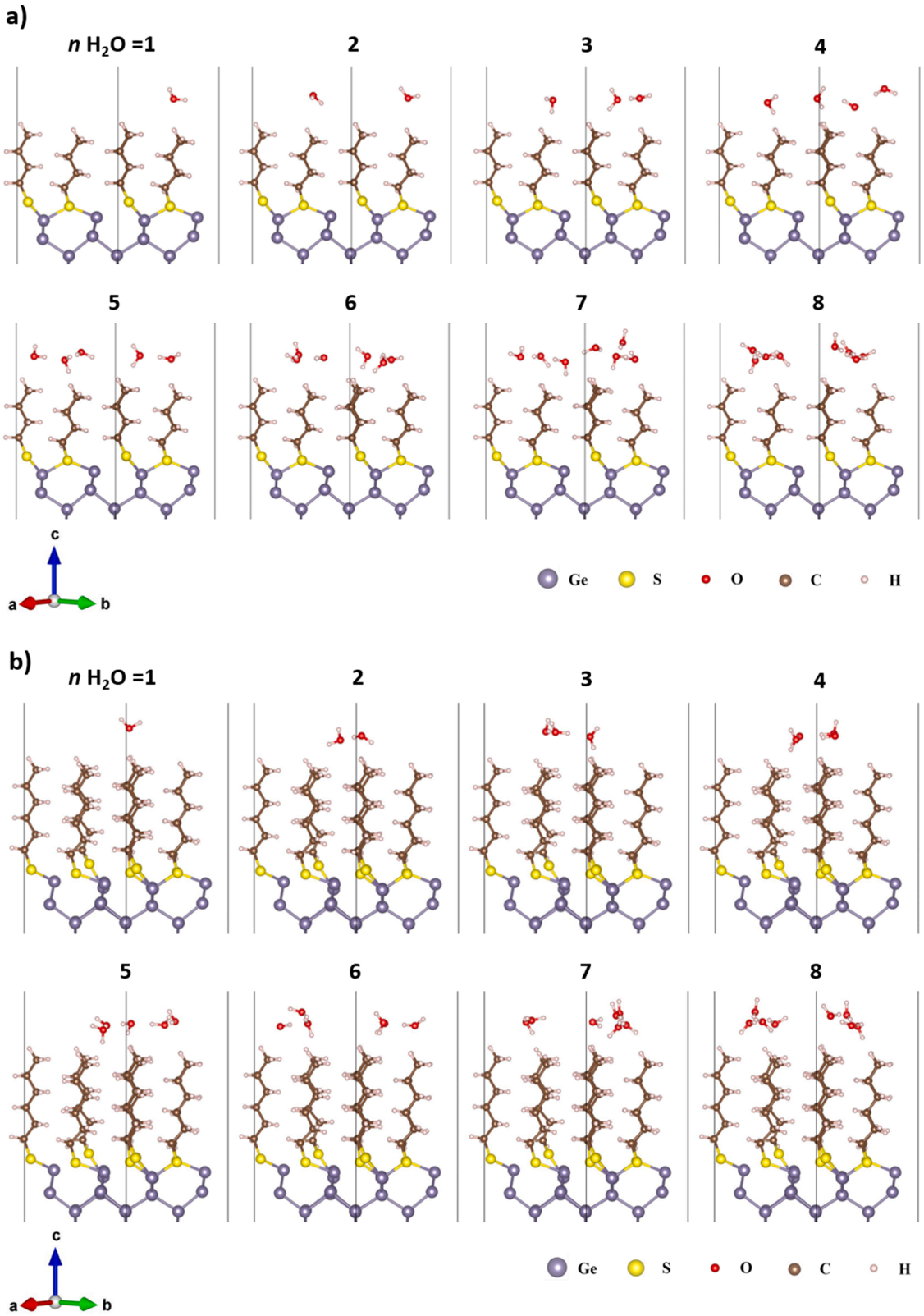

Fig. 10. Atomic structures of Ge(100) entirely covered by (a) butanethiol and (b) hexanethiol with n (1, …, 8) water molecules positioned on top of chains before the relaxation.

group in the thiolates, which repels the water molecules and is independent of the length of the thiolate chain.

The hydrophobic property of Ge(100) entirely covered by SAMs can be seen from the structures presented in Fig. 10. Water molecules are initially positioned to interact with the thiolates at the chain-vacuum interface and are repelled from the SAM after relaxation in both low and high water concentration scenarios.

In the case of a partially covered Ge surface, water molecules may

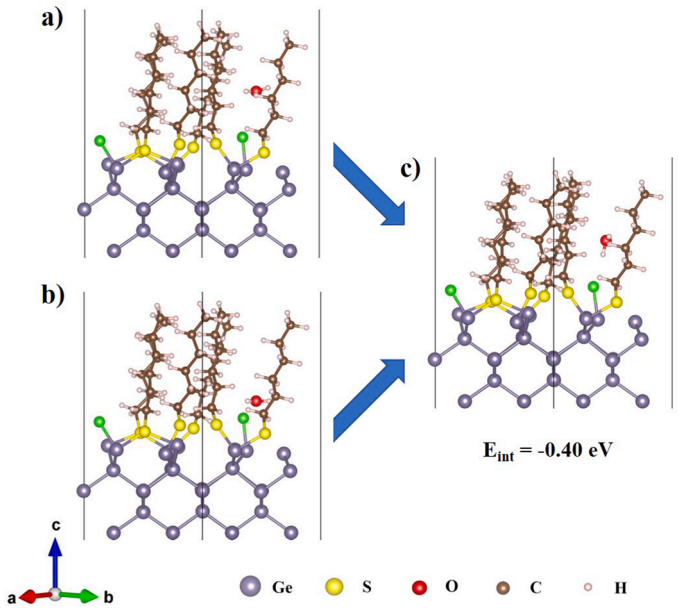

Fig. 11. Atomistic structure of Ge(100) with 75% hexanethiol coverage with a water molecule placed (a) in the middle of the chains and (b) near the Ge surface before the relaxation and (c) after relaxation.

migrate through any gaps between the chains but are still not able to easily reach the Ge surface because the SAM acts as a barrier, as demonstrated in the experimental work where Ge re-oxidation requires > 24 h. In Fig. 11, we show two initial configurations of a water molecule positioned in the space between thiol chains and near the Ge surface for hexanethiol SAMs at a surface coverage of 75%. After relaxation, both arrangements assume the same configuration with an interaction energy between water and the SAM-Ge system (E_{int}) of - 0.40 eV. Even if the water molecule is positioned near the thiolate-Ge interaction, it appears to relax away from the surface, trapped between two thiolate chains.

Interactions between water and a Ge surface passivated with butanethiol at 62.5% coverage as a function of water concentration are shown in Fig. 12. The SAM acts as a barrier at low water concentration where water molecules begin to be repelled by the chains as the number of water molecules increases. At highest water concentration, the water molecules are repelled by the terminating methyl group, as confirmed as confirmed by Howell et al.'s work on water–SAM interactions [63]. Calculated interaction energies of these structures are also reported in Fig. 12, as the number of water molecules increases, the interaction energy is always increasingly negative but interestingly, the interaction energy per molecule is higher at low concentration (n = 1, …, 4) than at high concentration (n = 5, …, 8), in which appears to be constant around -0.50 ± 0.05 eV.

For this SAM-Ge structure, we also investigated a range of initial configurations in which a water molecule that is present at the Ge-SAM interface can dissociate into one of two species. The first is the formation of a thiol molecule, with an S-H bond which migrates away from the surface and a surface Ge-OH bond. The second is formation of a HCl molecule which migrates from the surface and a surface Ge-OH bond; this can also promote Ge oxidation by removing the surface passivating Cl species, as illustrated in Fig. 13.

In the case of butanethiol passivated Ge at a thiolate coverage of 62.5% coverage, a dissociated water molecule relaxes to form a protonated HS-thiol molecule and a new Ge-OH bond with an interaction energy of -0.85 eV which is comparable to the configuration in which H_2O is not dissociated but interacts at the interface between the SAM and Ge, as shown in Fig. 14.

In Fig. 15, we show an example for the hexanethiol-Ge system at 62.5 % SAM coverage, where upon water dissociation, a HCl molecule is released and a Ge-OH species is formed. While this shows an apparently less favorable interaction energy of -0.19 eV compared to butanethiol, it is nonetheless competitive with the stability of a water molecule interacting at the SAM-Ge interface. This process removes the Cl species that passivates Ge in the absence of thiolates and also forms a new Ge-OH bond, which was proposed as the first step in re-oxidation of halide-passivated Ge in previous work [64].

We propose that re-oxidation can occur through two pathways, both involving water dissociation. One is the removal of Cl from the Ge surface as HCl and the other involves the removal of the SAM is as sketched in Fig. 13, while both result in Ge-OH at the surface.

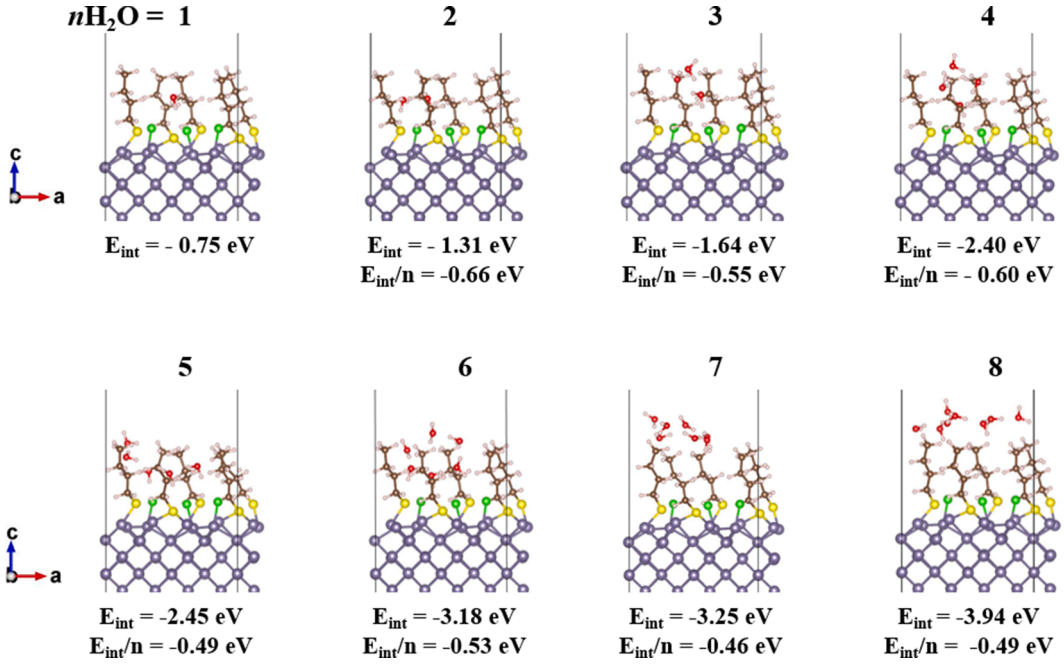

Fig. 12. Calculated adsorption energies and optimized structures of Ge(100) with 62.5% butanethiol coverage, with n (1, …, 8) water molecules.

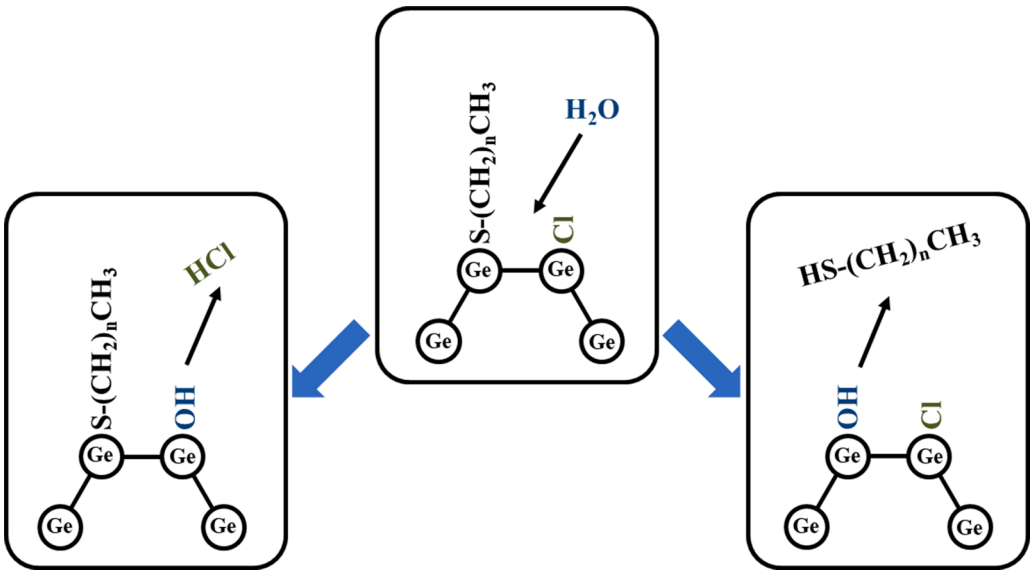

Fig. 13. Schematic indicating possible reaction pathways for water attacking Ge surface, both cases involving the displacement of a passivant by an OH group.

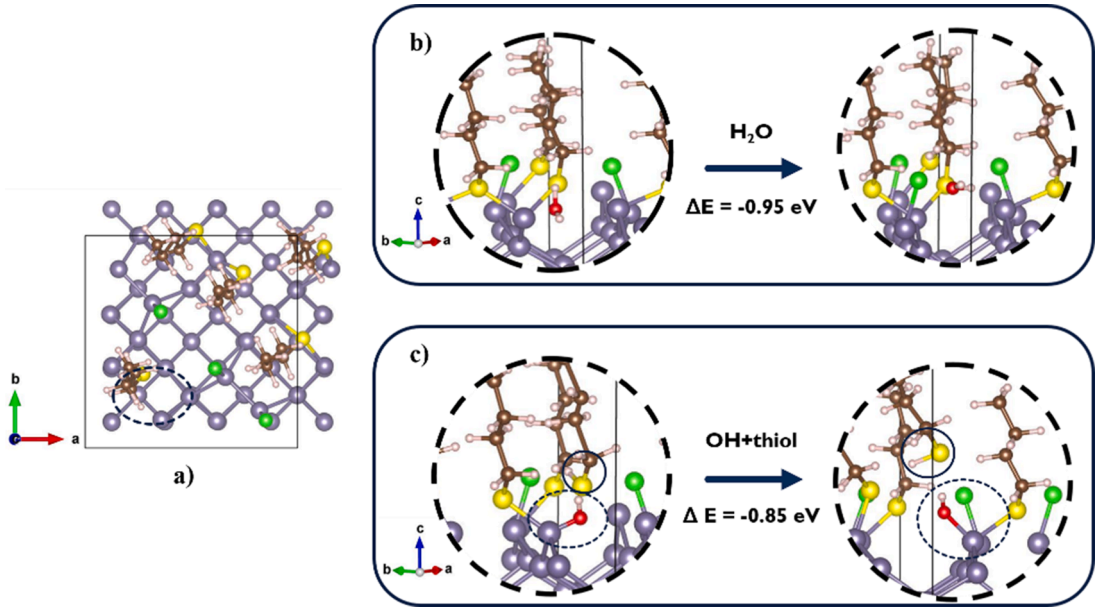

Fig. 14. (a) Model used to explore possible water dissociation in Ge(100) with butanethiol coverage of 62.5%, (b) a solution in which molecular water remains confined around the initial position, (c) water dissociation, in which water dissociates into hydrogen and hydroxide ions forming a Ge-OH bond and HS-thiol.

4. Conclusions

Given an industry requirement of a 24 h queue time for wafers during processing, the demonstration that there is a clear improvement in the longevity of alkanethiol passivated-Ge in low humidity environments is significant. By tracking the growth of native GeO_2 in time using XPS, the role that water vapor plays in SAM degradation and Ge surface oxidation is elucidated. The XPS results obtained indicate that higher humidity environments result in increased rates of oxidation of the thiol-passivated Ge surface. The WCA analysis complements these results wherein a greater decrease in contact angle is observed for the Ge samples exposed to the high humidity environment in contrast to those subjected to lower humidity environments. There are two potential avenues for SAM removal and Ge oxidation, (i) H_2O attacking the Ge-Cl bond, which are left over from the HCl etch, to form HCl and Ge-OH, and (ii) H_2O attacking the Ge-S-R bond to form R-SH and Ge-OH. This reaction paves the way for ambient oxygen to attack Ge-Ge bonds and further develop Ge oxide. [64] The methyl termination in the tail group plays a crucial role in acting as a barrier to water in the air, preventing water from migrating to the Ge-SAM interface. Oxidation that does occur is likely due to the presence of defect sites, which allow water to easily migrate to the surface. The experimental and modelling results highlight that by controlling the humidity of the environment the thiol-passivated Ge coupons are exposed to, the longevity of the SAM can be improved and thus the resistance to oxidation of the underlying Ge. Alternatively, improving the SAM can also have an impact on stability, for example by increasing the hydrophobicity of the tail group termination by using a fluorinated group, by increasing the chain alignment and packing density, or by decreasing the defect density. Given that Ge is predicted to be the channel material in future CMOS devices, methods to replace the complex and water-soluble native oxide will be required. SAMs are a likely candidate to perform this role as they

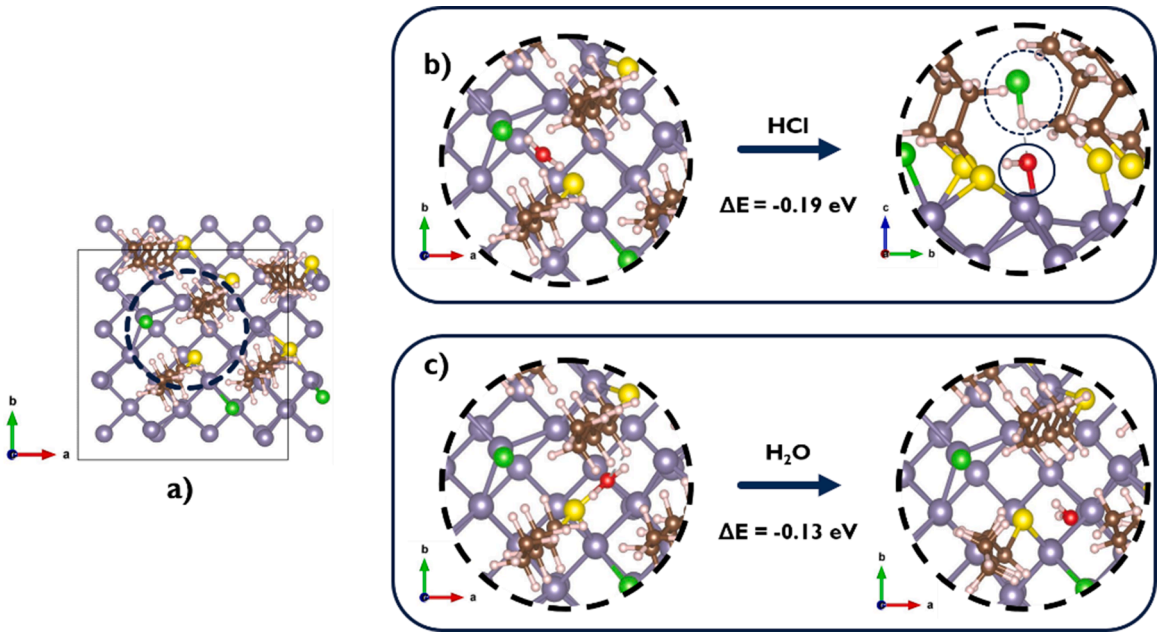

Fig. 15. (a) Model used to explore possible water dissociation in Ge(100) with hexanethiol coverage of 62.5%, (b) water dissociation, water breaks into hydrogen and hydroxide ions forming a Ge-OH bond and HCl molecule, (c) water remains confined around the initial position.

are easily applied so understanding how to improve their longevity is significant for queue time compliance.

Credit author statement

Shane Garvey: devised and carried out experimental procedures for the vapour phase passivation of Ge; carried out humidity tests in experimental chamber; carried out XPS measurements; co-wrote the manuscript. Andrew Serino: devised and carried out experimental procedures for the liquid and gas phase passivation of Ge; co-wrote the manuscript. Maria Barbara Maccioni: carried out the DFT calculations for the effect of humidity on passivated Ge; co-wrote the manuscript. Justin D. Holmes: provided input into the characterization of humidity results. Michael Nolan: carried out the DFT calculations for the effect of humidity on passivated Ge; co-wrote the manuscript. Nerissa Draeger: provided input into the characterization of humidity results. Emir Gruer: carried out XPS measurements on samples prepared in Fremont. Brenda Long: directed the research and provided input into the characterization of humidity results; co-wrote the manuscript.

Declaration of Competing Interest

The authors declare that they have no known competing financial interests or personal relationships that could have appeared to influence the work reported in this paper.

Data Availability

No data was used for the research described in the article.

Acknowledgments

BL, BM and MN acknowledge financial support from Enterprise Ireland (EI IP 20190757A & EI IP 20190757B) and access to computing resources at Irish Centre for High End Computing (ICHEC).

References

[1] S.R. Taylor, Abundance of chemical elements in the continental crust: a new table, Geochim. Cosmochim. Acta 28 (1964) 1273–1285, https://doi.org/10.1016/0016-7037(64)90129-2.
[2] K.E. Petersen, Silicon as a mechanical material, Proc. IEEE 70 (1982) 420–457, https://doi.org/10.1109/PROC.1982.12331.
[3] G. Pacchioni, L. Skuja, D. Griscom, Defects in SiO_2 and related dielectrics, Sci. Technol. (2000) 1–35, https://doi.org/10.1007/978-94-010-0944-7.
[4] G.D. Wilk, R.M. Wallace, J.M. Anthony, High-κ gate dielectrics: current status and materials properties considerations, J. Appl. Phys. 89 (2001) 5243–5275, https://doi.org/10.1063/1.1361065.
[5] M. Hirose, Electron tunneling through ultrathin SiO_2, Mater Sci. Eng. B Solid State Mater. Adv. Technol. 41 (1996) 35–38, https://doi.org/10.1016/S0921-5107(96)01619-4.
[6] J. Maserjian, N. Zamani, Behavior of the Si/SiO_2 interface observed by fowler-nordheim tunneling, J. Appl. Phys. 53 (1982) 559–567, https://doi.org/10.1063/1.329919.
[7] E.P. Gusev, D.A. Buchanan, E. Cartier, A. Kumar, D. DiMaria, S. Guha, A. Callegari, S. Zafar, P.C. Jamison, D.A. Neumayer, M. Copel, M.A. Gribelyuk, H. Okorn-Schmidt, C.D. Emic, P. Kozlowski, K. Chan, N. Bojarczuk, L. Ragnarsson, P. Ronsheim, K. Rim, R.J. Fleming, A. Mocuta, A. Ajmera, Ultrathin high-k gate stacks for advanced CMOS devices, in: Proceedings of the International Electron Devices Meeting, 2001, https://doi.org/10.1109/IEDM.2001.979537. Technical Digest (Cat. No.01CH37224)20.21.21-20.21.24.
[8] A. Gupta, T. Sakthivel, S. Seal, Recent development in 2D materials beyond graphene, Prog. Mater Sci. 73 (2015) 44–126, https://doi.org/10.1016/j.pmatsci.2015.02.002.
[9] K. Tomioka, M. Yoshimura, T. Fukui, A III–V nanowire channel on silicon for high-performance vertical transistors, Nature 488 (2012) 189–192, https://doi.org/10.1038/nature11293.
[10] G. Mirabelli, C. McGeough, M. Schmidt, E.K. McCarthy, S. Monaghan, I.M. Povey, M. McCarthy, F. Gity, R. Nagle, G. Hughes, A. Cafolla, P.K. Hurley, R. Duffy, Air sensitivity of MoS_2, $MoSe_2$, $MoTe_2$, HfS_2, and $HfSe_2$, J. Appl. Phys. 120 (2016), 125102, https://doi.org/10.1063/1.4963290.
[11] S. Manzeli, D. Ovchinnikov, D. Pasquier, O.V. Yazyev, A. Kis, 2D transition metal dichalcogenides, Nat. Rev. Mater. 2 (2017) 17033, https://doi.org/10.1038/natrevmats.2017.33.
[12] P. Crowson, Germanium, Miner. Handb. (1996) 5–12, https://doi.org/10.1007/978-1-349-06329-1_3.
[13] M.J.H.v. Dal, G. Vellianitis, G. Doornbos, B. Duriez, M.C. Holland, T. Vasen, A. Afzalian, E. Chen, S.K. Su, T.K. Chen, T.M. Shen, Z.Q. Wu, C.H. Diaz, Ge CMOS gate stack and contact development for vertically stacked lateral nanowire FETs, in: Proceedings of the EEE International Electron Devices Meeting (IEDM), 2018, https://doi.org/10.1109/IEDM.2018.8614577, 21.21.21-21.21.24.
[14] H. Shang, H. Okorn-Schimdt, J. Ott, P. Kozlowski, S. Steen, E.C. Jones, H.P. Wong, W. Hanesch, Electrical characterization of germanium p-channel MOSFETs, IEEE Electron Device Lett. 24 (2003) 242–244, https://doi.org/10.1109/LED.2003.810879.
[15] S. Huiling, L. Kam-Leung, P. Kozlowski, C.D. Emic, I. Babich, E. Sikorski, I. Meikei, H.P. Wong, K. Guarini, W. Haensch, Self-aligned n-channel germanium MOSFETs

with a thin Ge oxynitride gate dielectric and tungsten gate, IEEE Electron Device Lett. 25 (2004) 135–137, https://doi.org/10.1109/LED.2003.823060.
[16] S.C.A. Agrawal, W. Rachmady, S. Vishwanath, S. Ghose, M. Mehta, J. Torres, A.A. Oni, X. Weng, H. Li, D. Merrill, M. Metz, A. Murthy, J. Kavalieros, Gate-All-around strained Si0.4Ge0.6 nanosheet PMOS on strain relaxed buffer for high performance low power logic application, (2020), doi:10.1109/IEDM13553.2020.9371933.
[17] X. Luo, T. Nishimura, T. Yajima, A. Toriumi, Understanding of Fermi level pinning at metal/germanium interface based on semiconductor structure, Appl. Phys. Express 13 (2020), 031003, https://doi.org/10.35848/1882-0786/ab7713.
[18] T. Nishimura, K. Kita, A. Toriumi, Evidence for strong fermi-level pinning due to metal-induced gap states at metal/germanium interface, Appl. Phys. Lett. 91 (2007), 123123, https://doi.org/10.1063/1.2789701.
[19] A. Dimoulas, P. Tsipas, A. Sotiropoulos, E.K. Evangelou, Fermi-level pinning and charge neutrality level in germanium, Appl. Phys. Lett. 89 (2006), 252110, https://doi.org/10.1063/1.2410241.
[20] R.Rojas Delgado, R.M. Jacobberger, S.S. Roy, V.S. Mangu, M.S. Arnold, F. Cavallo, M.G. Lagally, Passivation of germanium by graphene, ACS Appl. Mater. Interfaces 9 (2017) 17629–17636, https://doi.org/10.1021/acsami.7b03889.
[21] J.R. Weber, A. Janotti, C.G. Van de Walle, Dangling bonds and vacancies in germanium, Phys. Rev. B 87 (2013), 035203, https://doi.org/10.1103/PhysRevB.87.035203.
[22] A. Toriumi, High electron mobility germanium (Ge) metal oxide semiconductor field effect transistors (MOSFETs), Silicon–Germanium (SiGe) Nanostructures (2011) 528–550, https://doi.org/10.1533/9780857091420.4.528.
[23] S.K. Wang, K. Kita, C.H. Lee, T. Tabata, T. Nishimura, K. Nagashio, A. Toriumi, Desorption kinetics of GeO From GeO_2/Ge structure, J. Appl. Phys. 108 (2010), 054104, https://doi.org/10.1063/1.3475990.
[24] D. Bodlaki, H. Yamamoto, D.H. Waldeck, E. Borguet, Ambient stability of chemically passivated germanium interfaces, Surf. Sci. 543 (2003) 63–74, https://doi.org/10.1016/S0039-6028(03)00958-0.
[25] X.J. Zhang, G. Xue, A. Agarwal, R. Tsu, M.A. Hasan, J.E. Greene, A. Rockett, Thermal desorption of ultraviolet–ozone oxidized Ge(001) for substrate cleaning, J. Vac. Sci. Technol. A 11 (1993) 2553–2561, https://doi.org/10.1116/1.578606.
[26] M.W.C. Dharma-wardana, M.Z. Zgierski, D. Ritchie, J.G. Ping, H. Ruda, Comparison of cluster and slab models of the surface structure of Cl-terminated Ge (111) and GaAs(111) surfaces, Phys. Rev. B 59 (1999) 15766–15771, https://doi.org/10.1103/PhysRevB.59.15766.
[27] A. Molina, J.R. Shallenberger, S.E. Mohney, Vapor phase passivation of (100) germanium surfaces with HBr, J. Vac. Sci. Technol. A 38 (2020), 023208, https://doi.org/10.1116/1.5141941.
[28] G.H.A. Abrenica, M.V. Lebedev, G. Okorn, D.H. van Dorp, M. Fingerle, Wet-chemical bromination of Ge (100): a facile surface passivation tool, Appl. Phys. Lett. 113 (2018), 062104, https://doi.org/10.1063/1.5044512.
[29] M.A. Filler, J.A. Van Deventer, A.J. Keung, S.F. Bent, Carboxylic acid chemistry at the Ge(100)-2 × 1 interface: bidentate bridging structure formation on a semiconductor surface, J. Am. Chem. Soc. 128 (2006) 770–779, https://doi.org/10.1021/ja0549502.
[30] J. Roche, P. Ryan, G.J. Hughes, Core level photoemission studies of the sulphur terminated Ge(100) surface, Appl. Surf. Sci. 174 (2001) 271–274, https://doi.org/10.1016/S0169-4332(01)00172-6.
[31] G. Maggioni, S. Carturan, L. Fiorese, N. Pinto, F. Caproli, D.R. Napoli, M. Giarola, G. Mariotto, Germanium nitride and oxynitride films for surface passivation of Ge radiation detectors, Appl. Surf. Sci. 393 (2017) 119–126, https://doi.org/10.1016/j.apsusc.2016.10.006.
[32] H. Kim, P.C. McIntyre, C.O. Chui, K.C. Saraswat, M.-H. Cho, Interfacial characteristics of HfO_2 grown on nitrided Ge (100) substrates by atomic-layer deposition, Appl. Phys. Lett. 85 (2004) 2902–2904, https://doi.org/10.1063/1.1797564.
[33] G.P. Campbell, B. Kiraly, R.M. Jacobberger, A.J. Mannix, M.S. Arnold, M. C. Hersam, N.P. Guisinger, M.J. Bedzyk, Epitaxial graphene-encapsulated surface reconstruction of Ge(110), Phys. Rev. Mater. 2 (2018), 044004, https://doi.org/10.1103/PhysRevMaterials.2.044004.
[34] B. Kiraly, R.M. Jacobberger, A.J. Mannix, G.P. Campbell, M.J. Bedzyk, M.S. Arnold, M.C. Hersam, N.P. Guisinger, Electronic and mechanical properties of graphene–germanium interfaces grown by chemical vapor deposition, Nano Lett. 15 (2015) 7414–7420, https://doi.org/10.1021/acs.nanolett.5b02833.
[35] G. Collins, D. Aureau, J.D. Holmes, A. Etcheberry, C. O'Dwyer, Germanium oxide removal by citric acid and thiol passivation from citric acid-terminated Ge(100), Langmuir 30 (2014) 14123–14127, https://doi.org/10.1021/la503819z.
[36] S. Garvey, J.D. Holmes, Y.S. Kim, B. Long, Vapor-phase passivation of chlorine-terminated Ge(100) using self-assembled monolayers of hexanethiol, ACS Appl. Mater. Interfaces 12 (2020) 29899–29907, https://doi.org/10.1021/acsami.0c02548.
[37] C.D. Bain, H.A. Biebuyck, G.M. Whitesides, Comparison of self-assembled monolayers on gold: coadsorption of thiols and disulfides, Langmuir 5 (1989) 723–727, https://doi.org/10.1021/la00087a027.
[38] D.S. Bergsman, T.L. Liu, R.G. Closser, K.L. Nardi, N. Draeger, D.M. Hausmann, S. F. Bent, Formation and ripening of self-assembled multilayers from the vapor-phase deposition of dodecanethiol on copper oxide, Chem. Mater. 30 (2018) 5694–5703, https://doi.org/10.1021/acs.chemmater.8b02150.
[39] C.K. Kanukula, A. Boyapati, Y. Md Iqbal, S. Bojja, Corrosion protection of copper by self assembled monolayers, Indian J. Chem. Technol. 16 (2009) 25–31.
[40] G. Alessio Verni, B. Long, F. Gity, M. Lanius, P. Schüffelgen, G. Mussler, D. Grützmacher, J. Greer, J.D. Holmes, Oxide removal and stabilization of bismuth thin films through chemically bound thiol layers, RSC Adv. 8 (2018) 33368–33373, https://doi.org/10.1039/C8RA06840B.
[41] B. Long, M. Manning, M. Burke, B.N. Szafranek, G. Visimberga, D. Thompson, J. C. Greer, I.M. Povey, J. MacHale, G. Lejosne, D. Neumaier, A.J. Quinn, Non-covalent functionalization of graphene using self-assembly of alkane-amines, Adv. Funct. Mater. 22 (2012) 717–725, https://doi.org/10.1002/adfm.201101956.
[42] D. Zerulla, T. Chassé, Structure and self-assembly of alkanethiols on III–V semiconductor (110) surfaces, J. Electron Spectrosc. Relat. Phenom. 172 (2009) 78–87, https://doi.org/10.1016/j.elspec.2009.03.017.
[43] A.J. Muscat, Self-assembly of functionalized organic molecules on flat solid surfaces, Encycl. Interfacial Chem. (2018) 810–816, https://doi.org/10.1016/B978-0-12-409547-2.13137-3. Encycl. Interfacial Chem.
[44] M. Singh, N. Kaur, E. Comini, The role of self-assembled monolayers in electronic devices, J. Mater. Chem. C 8 (2020) 3938–3955, https://doi.org/10.1039/D0TC00388C.
[45] M. Takenaka, K. Morii, M. Sugiyama, Y. Nakano, S. Takagi, Gas phase doping of arsenic into (100), (110), and (111) germanium substrates using a metal–organic source, Jpn. J. Appl. Phys. 50 (2011), 010105, https://doi.org/10.1143/jjap.50.010105.
[46] N. Kennedy, S. Garvey, B. Maccioni, L. Eaton, M. Nolan, R. Duffy, F. Meaney, M. Kennedy, J.D. Holmes, B. Long, Monolayer doping of germanium with arsenic: a new chemical route to achieve optimal dopant activation, Langmuir 36 (2020) 9993–10002, https://doi.org/10.1021/acs.langmuir.0c00408.
[47] F. Sgarbossa, S.M. Carturan, D.D. Salvador, G.A. Rizzi, E. Napolitani, G. Maggioni, W. Raniero, D.R. Napoli, G. Granozzi, A. Carnera, Monolayer doping of germanium by phosphorus-containing molecules, Nanotechnology 29 (2018), 465702, https://doi.org/10.1088/1361-6528/aade30.
[48] F. Sgarbossa, G. Maggioni, G.A. Rizzi, S.M. Carturan, E. Napolitani, W. Raniero, C. Carraro, F. Bondino, I. Píš, D. De Salvador, Self-limiting Sb monolayer as a diffusion source for Ge doping, Appl. Surf. Sci. 496 (2019), 143713, https://doi.org/10.1016/j.apsusc.2019.143713.
[49] C.M. Wolff, L. Canil, C. Rehermann, N. Ngoc Linh, F. Zu, M. Ralaiarisoa, P. Caprioglio, L. Fiedler, M. Stolterfoht, S. Kogikoski, I. Bald, N. Koch, E.L. Unger, T. Dittrich, A. Abate, D. Neher, Perfluorinated self-assembled monolayers enhance the stability and efficiency of inverted perovskite solar cells, ACS Nano 14 (2020) 1445–1456, https://doi.org/10.1021/acsnano.9b03268.
[50] E. Yalcin, M. Can, C. Rodriguez-Seco, E. Aktas, R. Pudi, W. Cambarau, S. Demic, E. Palomares, Semiconductor self-assembled monolayers as selective contacts for efficient PiN perovskite solar cells, Energy Environ. Sci. 12 (2019) 230–237, https://doi.org/10.1039/C8EE01831F.
[51] D. Mandler, S. Kraus-Ophir, Self-assembled monolayers (SAMs) for electrochemical sensing, J. Solid State Electrochem. 15 (2011) 1535, https://doi.org/10.1007/s10008-011-1493-6.
[52] J.N. Hohman, M. Kim, H.R. Bednar, J.A. Lawrence, P.D. McClanahan, P.S. Weiss, Simple, robust molecular self-assembly on germanium, Chem. Sci. 2 (2011) 1334–1343, https://doi.org/10.1039/C1SC00115A.
[53] D. Wang, Y.L. Chang, Z. Liu, H. Dai, Oxidation resistant germanium nanowires: bulk synthesis, long chain alkanethiol functionalization, and langmuir-blodgett assembly, J. Am. Chem. Soc. 127 (2005) 11871–11875, https://doi.org/10.1021/ja053836g.
[54] Q. Cai, B. Xu, L. Ye, Z. Di, S. Huang, X. Du, J. Zhang, Q. Jin, J. Zhao, 1-dodecanethiol based highly stable self-assembled monolayers for germanium passivation, Appl. Surf. Sci. 353 (2015) 890–901, https://doi.org/10.1016/j.apsusc.2015.06.174.
[55] G. Kresse, J. Furthmüller, Efficiency of *ab-initio* total energy calculations for metals and semiconductors using a plane-wave basis set, Comput. Mater. Sci. 6 (1996) 15–50, https://doi.org/10.1016/0927-0256(96)00008-0.
[56] G. Kresse, J. Furthmüller, Efficient iterative schemes for *ab-initio* total-energy calculations using a plane-wave basis set, Phys. Rev. B 54 (1996) 11169–11186, https://doi.org/10.1103/PhysRevB.54.11169.
[57] P.E. Blöchl, Projector augmented-wave method, Phys. Rev. B 50 (1994) 17953–17979, https://doi.org/10.1103/PhysRevB.50.17953.
[58] J.P. Perdew, K. Burke, M. Ernzerhof, Generalized gradient approximation made simple, Phys. Rev. Lett. 77 (1996) 3865–3868, https://doi.org/10.1103/PhysRevLett.77.3865.
[59] S. Grimme, J. Antony, S. Ehrlich, H. Krieg, A Consistent and accurate ab-initio parametrization of density functional dispersion correction (DFT-D) for the 94 elements H-Pu, J. Chem. Phys. 132 (2010), 154104, https://doi.org/10.1063/1.3382344.
[60] H.J. Monkhorst, J.D. Pack, Special points for brillouin-zone integrations, Phys. Rev. B 13 (1976) 5188–5192, https://doi.org/10.1103/PhysRevB.13.5188.
[61] H. Murakami, T. Fujioka, A. Ohta, T. Bando, S. Higashi, S. Miyazaki, Characterization of interfaces between chemically cleaned or thermally oxidized germanium and metals, 33 (2010) 253, doi:10.1149/1.3487556.
[62] J. Bal, S. Kundu, S. Hazra, Hydrophilic-like wettability of Cl-passivated Ge(001) surface, Chem. Phys. 406 (2012) 72, https://doi.org/10.1016/j.chemphys.2012.08.010.
[63] C. Howell, R. Maul, W. Wenzel, P. Koelsch, Interactions of hydrophobic and hydrophilic self-assembled monolayers with water as probed by sum-frequency-generation spectroscopy, Chem. Phys. Lett. 494 (2010) 193–197, https://doi.org/10.1016/j.cplett.2010.06.008.
[64] S. Sun, Y. Sun, Z. Liu, D.I. Lee, P. Pianetta, Roles of oxygen and water vapor in the oxidation of halogen terminated Ge(111) surfaces, Appl. Phys. Lett. 89 (2006), 231925, https://doi.org/10.1063/1.2403908.